Integrated line-of-sight modeling of the Airborne Aero-Optics Laboratory

Steven Griffin and John Blackburn

The Boeing Company

James Thordahl

The Aerospace Corporation

Donald Wittich

Air Force Research Laboratory

Stanislav Gordeyev and Eric Jumper

University of Notre Dame

1. ABSTRACT

The Airborne Aero-Optics Laboratory (AAOL) was designed to measure the effects of turbulent flow on the wavefront of a laser projected from an airplane in flight. An integrated line-of-sight model that predicts closed-loop jitter of the AAOL system is presented. The influence of model uncertainty with model tuning based on available experimental measurements was examined for one flight condition.

2. INTRODUCTION

The Airborne Aero-Optics Laboratory (AAOL) is a recently completed research platform to measure the effects of turbulent flow on the wavefront of a laser projected from an airplane in flight. The flight-test system consists of two Cessna Citation Bravo aircraft flying in formation at a distance of approximately 50 m. One aircraft projects a laser beam to the other aircraft which receives the beam as shown in Fig. 1. The beam is received by the pointing and stabilization component of AAOL, which includes an inertially stabilized azimuth and elevation turret and a high bandwidth track loop that uses a fast steering mirror to stabilize the incoming beam.

Fig. 1 Flight-Test System [1]

The interior of the AAOL cabin contains high speed wavefront sensing and data collection as shown in Fig. 2.

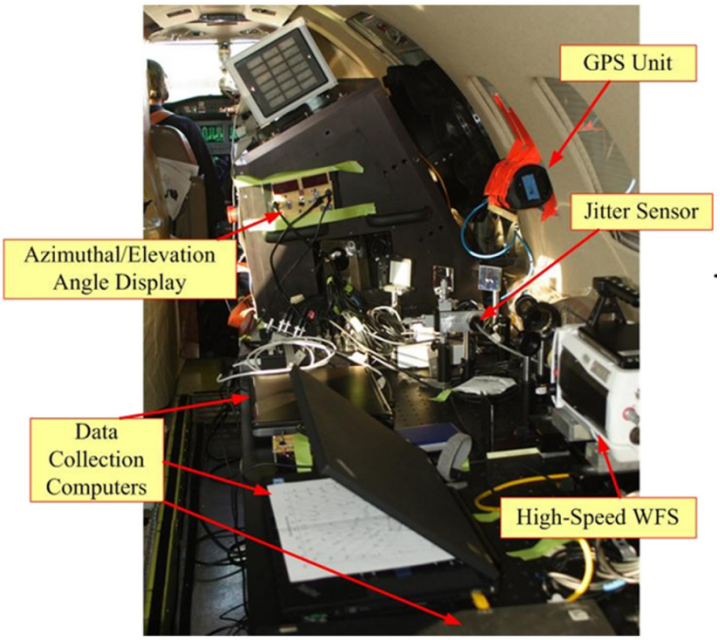

Fig. 2 –AAOL cabin interior [1]

In addition to providing a means for understanding and correcting optical wavefront distortion due to turbulence, AAOL also provides an ideal platform for predicting line-of-sight jitter and comparing it to measured results. AAOL has the essential elements of an airborne optical beam control system and is subject to relevant aero-loading, but operates at low power and provides a relatively inexpensive platform for collecting flight data.

This paper presents the integrated line-of-sight model of the pointing and tracking portion of AAOL for prediction of optical jitter due to flight disturbances. To accomplish this, an integrated line-of-sight model was derived from a finite element model of the system, optical sensitivities and control loops for calculation of closed loop, line-of-sight jitter. Disturbance inputs include measured in-flight base loading and measured pressure. The influence of model uncertainty was also addressed by considering two separate models. Model 1 used only information available from the initial hardware design before hardware assembly. Model 2 was updated based on modal tests performed on the assembled flight hardware. Frequency-varying model uncertainty factors (MUFs) for both models required to accurately predict the measured flight data were calculated. A slightly modified definition of MUFs is presented to calculate lower and upper bounds of uncertainty of a deterministic prediction.

3. ANALYSIS MODEL

The finite element model of the AAOL pointing and tracking system is shown in Fig. 3. The turret has a graphite/epoxy shell with its primary stiffness derived from an aluminum interior structure. Azimuth and elevation axis bearings are modeled using manufacturer's stiffness values. The fast steering mirror and all optical components are modeled explicitly although

mirror resonances are out of the bandwidth of interest in this analysis. Bonds between the optics and mounts are also modeled explicitly and were important in capturing the behavior of the fast steering mirror at high frequencies. The finite element model was constructed using FEMAP with NX NASTRAN as the solver. The model included 385194 nodes and 244464 elements. A modal analysis was conducted to extract mode shapes and frequencies to construct a state space modal using mode superposition [2].

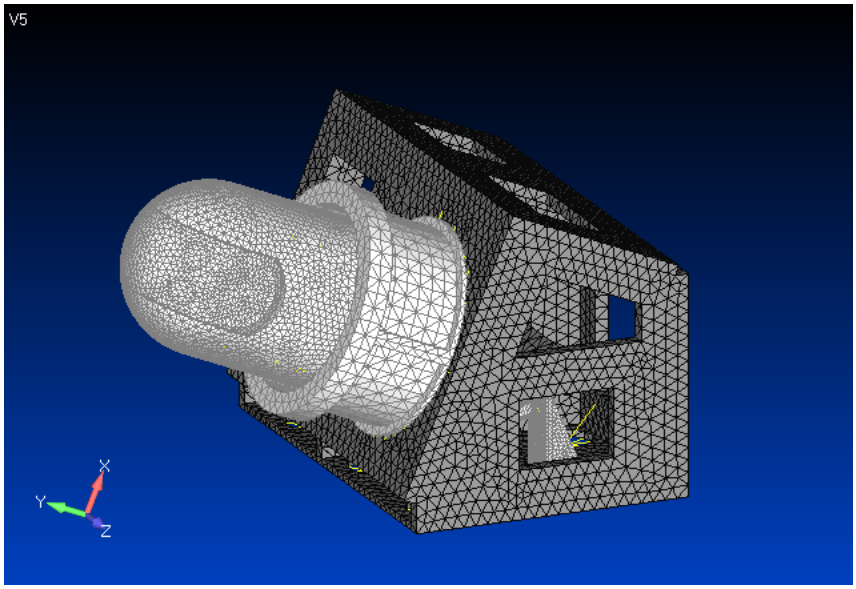

Fig. 3 – Finite element model of pointing and tracking system

The state space model was assembled in Matlab/Simulink. Within Simulink, modal damping was added based on measured data as well as increased damping of the primary that resulted from a targeted damping treatment. The inputs to the state space model were

1) Pressure on the turret
2) Base disturbance data in six degrees of freedom
3) Input torques to fast steering mirror
4) Input torques to azimuth and elevation axis

The outputs of the state space model were

1) Motion of twelve optical surfaces in 6 degrees of freedom
2) Azimuth and elevation angles

Control loops on the azimuth, elevation and fast steering mirror were also implemented in Simulink. Optical sensitivities were derived from the system optical prescription shown in Fig. 4 that related the six degree-of-freedom motion of each optical surface to jitter in output space. The resulting vectors, when multiplied by motion of the optics, gave two-axis jitter in output space as an additional output of the state space model. The resulting line-of-sight model was capable of predicting closed loop jitter due to measured base and pressure disturbances. The

same approach can also be used to predict dynamic optical wavefront distortion due to relative motion of figured optics, although this was not a desired output of this study.

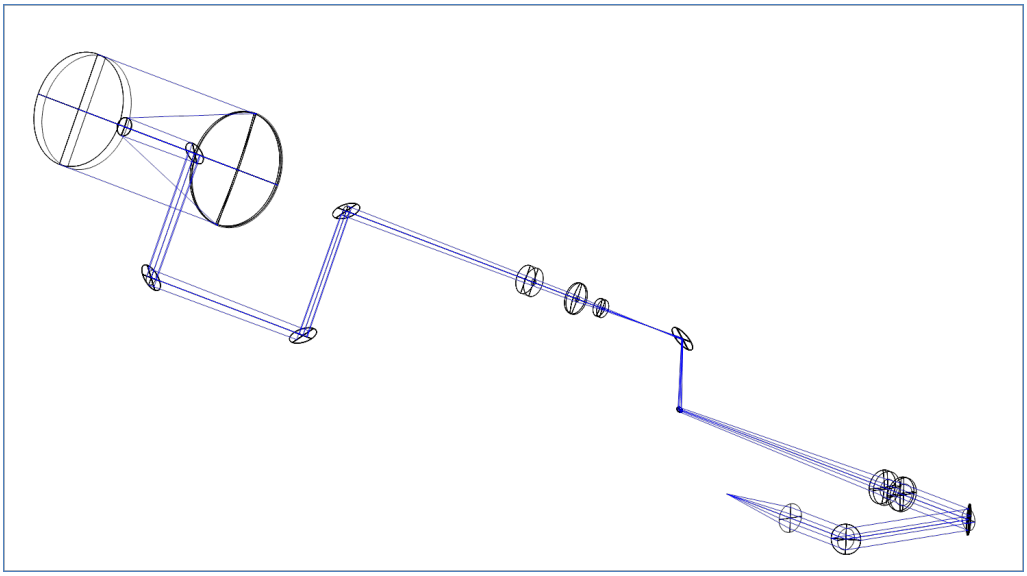

Fig. 4 – Optical path of AAOL pointing and tracking system

In order to study the impact on model tuning on closed loop jitter prediction, two model configurations were considered. Model 1 was intended to be representative of an optical system where best practices were used to assemble the finite element model and line-of-sight model but the hardware was not completed and thus not available for testing. Model 2 used Model 1 as a starting point, but components were tuned based on modal testing and other available data from the hardware. Structural parameters tuned in Model 2 were

1) Frequency and damping of the primary mirror
2) Bending frequencies of turret on azimuth bearing
3) Frequencies of optical components accessible via modal test

Ideally, all of the optics would have been tuned in Model 2. However, aside from the primary mirror, only four of the optics were accessible. The secondary mirror, which was figured and had significant sensitivity in all six degrees of freedom, was not accessible.

In addition, the high bandwidth control loop was implemented differently in Models 1 and 2. Similar to the structural parameters, it was assumed that the exact configuration of the controller was not known for Model 1, but the requirement was given as 500 Hz bandwidth based on the 0 dB crossover of the open-loop plant. The control architecture selected to achieve this goal was a broken integrator in series with a lead at crossover as shown in Fig. 5.

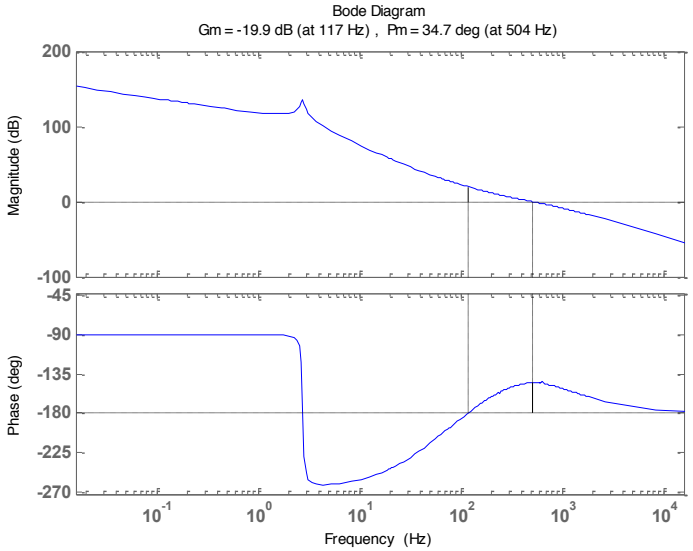

Fig. 5 – Model 1 – Control loop configuration

The control approach in Model 2 took advantage of transfer function measurements of the actual high bandwidth controller implemented on AAOL. A PID control approach was selected with a band-limited differentiator to match the measured closed-loop compensator. The PID coefficients were adjusted to match the measured behavior. The measured and tuned results are shown in Fig. 6.

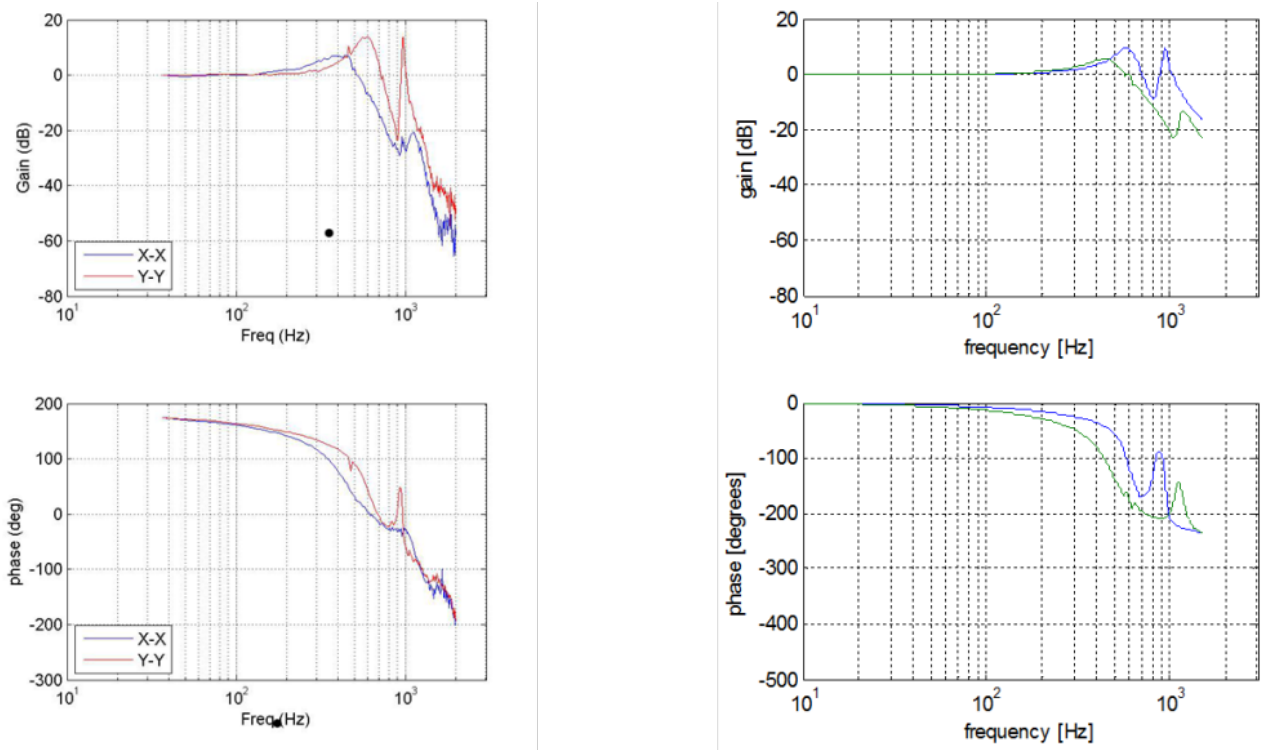

Measured Tuned

Fig. 6 – Measured and tuned compensator results

The large gain in the closed-loop transfer function measurement in the Y-Y direction at approximately 600 Hz is indicative of mistuning in the controller that was implemented in the AAOL flight experiment for this flight condition. Unlike the more well-behaved X-X direction, the gain was higher than desired in the Y-Y direction causing a large amplification at 600 Hz when the loop was closed. This high gain also resulted in a very lightly damped peak in the Y-Y direction transfer function at around 1000 Hz, which was believed to be due to the controller destabilizing a vibration mode of the fast steering mirror optic. In the updated finite element model, the mode at this frequency clearly displayed relative motion between the optic and the fast steering mirror housing with significant strain energy in the bond between them. As with the measured data, this mode is destabilized in the tuned model as shown in Figure 6 with the PID compensator.

The disturbances used for both Models 1 and 2 included a measured six degree of freedom base disturbance and measured pressure loading on the turret. Fig. 7 shows the angular and linear base disturbances derived from accelerometer and gyroscope measurements of the Cessna aircraft.

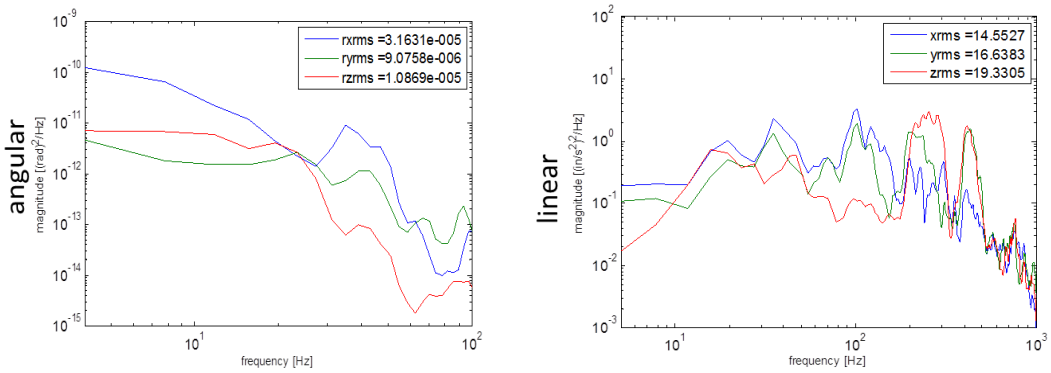

Fig. 7 – Measured angular and linear disturbances

The distributed pressure disturbances were extracted from pressure sensitive paint applied to the turret [3]. The measurement provided a time-varying pressure at the nodes on the exposed surface of the turret. The resulting predicted and measured two-axis jitter power spectrums at a representative flight condition are shown in Fig. 8.

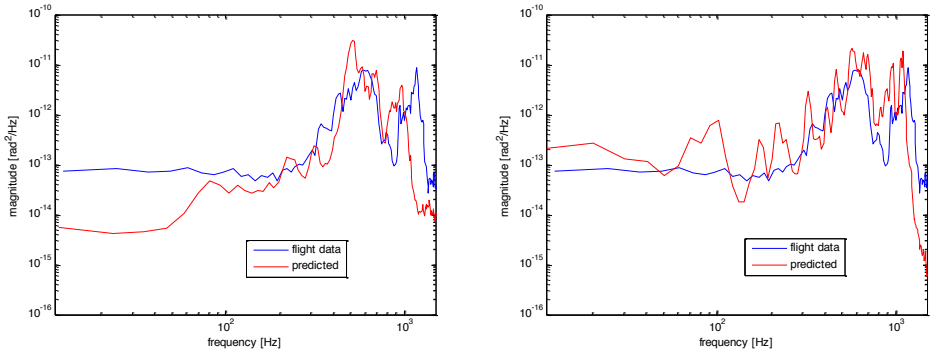

Model 1 Model 2

Fig. 8 - Measured and predicted jitter for Models 1 and 2

Both models qualitatively predict the measured closed-loop flight jitter power spectrums with the majority of the contribution at two high frequency "peaks". To further quantify the comparison, the power spectrum was broken into third octaves and the RMS jitter was calculated for each division. The resulting measurement is shown in Fig. 9 along with the flight data.

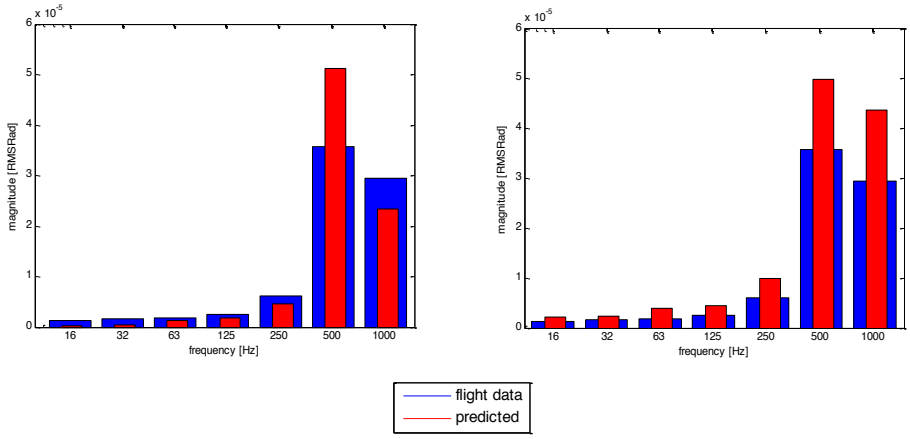

Model 1 Model 2

Fig. 9 – Third octave measurements for Models 1 and 2

The third octave measurement shows that Model 2 gives uniformly conservative predictions over all bands while Model 1 gives a conservative prediction in the most important band centered at 500 Hz, but is not conservative in all other bands.

4. MODEL UNCERTAINTY FACTORS

Model uncertainty factors [MUFS] are used to add conservatism to jitter prediction of an electro-optical system [4], usually before the hardware is assembled. One advantage of MUFS is the recognition that uncertainty can be frequency dependent, usually with increasing factors at higher frequencies. For models based on finite element results, this is consistent with decreasing confidence in predictions with increasing frequency and/or modal density. Typically, MUFS are applied over broader frequency ranges than third octaves and are significantly larger than would be needed to account for differences shown in Fig. 9. For example, Uebelhart [5] gives two frequency bands with factors of 4 and 20. In applying MUFS, rms (root mean square) jitter results from a deterministic analysis in each frequency band are multiplied by corresponding MUFS to give an upper bound that is expected to envelope the behavior of the assembled hardware. The corresponding lower bound of uncertainty is not calculated, since the goal is to add conservatism to the prediction. In the case of AAOL, predictions and hardware measurements were available, so the values of MUFs necessary to insure that the predicted results envelope the measured flight results for Models 1 and 2 could be calculated and compared. Since Model 2 gave consistently conservative results, the traditional definition of MUFs was altered slightly to also consider the lower bound of uncertainty. The upper bound remains $UB_i = \theta_i MUF_i$ where θ_i is the predicted rms jitter in the ith band and MUF_i is the corresponding multiplication factor. Additionally, a lower bound is introduced as $LB_i = \theta_i(2 - MUF_i)$ when $1 < MUF_i < 2$. Assuming all of the predicted results are either at a lower

bound or an upper bound in Fig. 9, it is then possible to calculate MUFs necessary to envelope the measured data. These results are shown in Fig. 10 with the results in green using the lower bound equation to derive the MUF and the results in red using the upper bound equation.

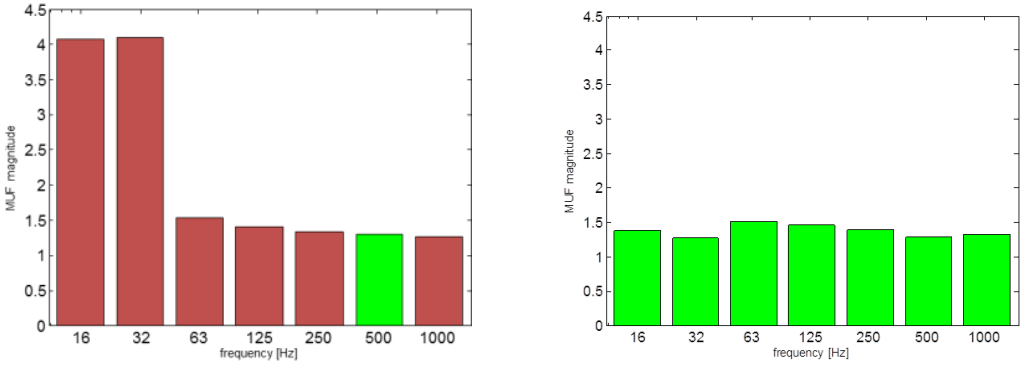

Fig. 10 – Calculated MUFs for Models 1 and 2

The updates in Model 2 clearly served to reduce the value of the MUFs, as redefined. If the more traditional value of only requiring the model times the MUF to give a conservative estimate in each band, all of the MUFs for Model 2 would be equal to 1 and an even greater decrease would be apparent. The largest decrease was in the frequency bands centered at 16 and 32 Hz. The reason for the relatively large MUFs in Model 1 in these bands was the difference in control architectures. The Model 1 control architecture had better low frequency rejection than the controller that was implemented on the hardware. Since the specification for the hardware only gave bandwidth and not low frequency behavior, this difference might be expected. The corresponding decrease in Model 2 MUFs in these bands reflects the update to the controller matching the actual performance of the controller at low frequency. The two-axis jitter forward sums derived from the power spectrums of Fig. 8 are shown in Fig. 11.

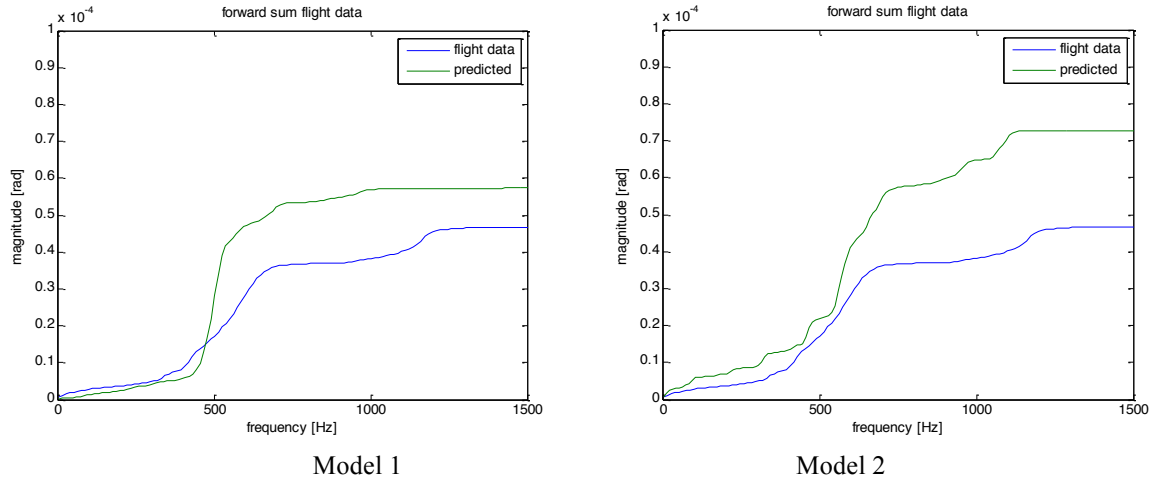

Fig. 11 – Forward Sums for Models 1 and 2 and Flight Data

Even though tuning the model significantly decreased the MUFs overall, the Model 1 two-axis jitter result was closer to the measured result. One possible explanation for this is that the frequency bands where the MUFs were greatly decreased centered at 16 and 32 were not a large contributor to overall jitter. Also, the uniform conservatism of Model 2 did not allow for any cancelling out of errors, with a conservative result in one frequency band being offset by a nonconservative result in another frequency band.

5. CONCLUSION

An integrated line-of-sight model was presented that predicts closed-loop jitter of the AAOL system. The impact of updating the model with available modal test data and transfer function data were assessed for one flight condition. Given the complexity of the system, the agreement between modeled and measured data was relatively good, based on a comparison of MUFs used in the literature. The exceptions were frequency bands in Model 1 that were not important in the prediction of overall jitter. It was not obvious that updating the model as described had a clear benefit in predicting jitter other than to insure conservatism in all frequency bands.

6. BIBLIOGRAPHY

[1] E. Jumper, M. Zenk, S. Gordeyev, D. Cavalieri and M. Whiteley, "The Airborne Aero-Optics Laboratory, AAOL," *Optical Engineering,* vol. 52, no. 7, 2013.

[2] K. Huebner, D. Dewhirst, D. Smith and T. Byrom, The Finite Element Method for Engineers, NY: John Wiley and Sons, 2001.

[3] N. DeLucca, E. Gordeyev, E. Jumper, K. Hird, T. Juliano, J. Gregory and D. Wittich, "The Estimation of the Unsteady Aerodynamic Force Applied to a Turret in Flight," *to be presented at 43rd AIAA Fluid Dynamics Conference and Exhibit*, San Diego, 2013.

[4] K. O' Keefe, "Dynamic Modeling Methodology," in *International Conference on Space Optical Systems and Applications*, Santa Monica, 2011.

[5] S. Uebelhart, D. Miller and C. Blaurock, "Uncertainty Characterization in Integrated Modeling," in *46th AIAA/ASME/ASCE/AHS/ASC Structures, Structural Dynamics and Materials Conference*, Austin, 2005.